Korean J. Chem. Eng., 37(2), 209-215 (2020)
DOI: 10.1007/s11814-019-0419-3

pISSN: 0256-1115
eISSN: 1975-7220

Efficient removal of the carbon deposits formed during the mixed methane reforming over Ni/Al_2O_3

Oleksandr Shtyka*,†, Mateusz Zakrzewski*, Radoslaw Ciesielski*, Adam Kedziora*, Sergey Dubkov, Roman Ryazanov***, Malgorzata Szynkowska*, and Tomasz Maniecki***

*Institute of General and Ecological Chemistry, Lodz University of Technology, Zeromskiego 116, 90-924 Lodz, Poland
**National Research University of Electronic Technology, Institute of Advanced Materials and Technologies, Shokin Square 1, 124498, Zelenograd, Moscow, Russia
***Scientific-Manufacturing Complex "Technological Centre", 1-7 Shokin Square, 124498, Zelenograd, Moscow, Russia
(*Received 12 July 2019 • accepted 3 November 2019*)

Abstract−This work investigates the process of elimination of carbon deposits formed during the mixed reforming of methane mixture. The mixed reforming of methane to synthesis gas was studied over Ni/Al_2O_3 catalyst in the 650-750 °C. The amount of carbon deposit on the surface of catalyst varied from 2.8 to 5.9%, depending on the reaction temperature. The reactivity of carbon species was evaluated in the oxygen, hydrogen, carbon dioxide, and water mixtures. The obtained results revealed the presence of highly active carbon form (etched at a temperature below 200 °C) and inactive form (gasification at a temperature above 500 °C). The SEM and Raman analyses confirmed the presence of carbon in the form of filaments. Among all investigated gasification agents, water vapor was found to be the most efficient in removing the carbon deposit due to better adsorption of water on the surface of aluminum oxide. The overall mechanism of mixed methane reforming along with carbon gasification was shown.

Keywords: Methane Reforming, Carbon Deposit, Nickel Catalyst, Gasification, Reaction Mechanism

INTRODUCTION

Biogas is among the most promising alternative options for decreasing greenhouse emissions and ensuring the security of the energy supply. Being the product of waste biomass anaerobic digestion, it consists mainly of methane and carbon dioxide, and therefore can be processed to syngas via dry reforming of methane. Industrially, this process is typically carried out under atmospheric pressure and temperatures of 700-900 °C in the presence of Ni/Al_2O_3 catalyst [1]. The main obstacle preventing the widespread application of this process to volume production is the rapid deactivation of catalysts due to rapid carbon deposition and sintering of metal particles. Therefore, much effort has been devoted to the development of more stable catalysts for this reaction [2]. Most of them are based on noble metals which are less susceptible to coking than the nickel-based catalysts. However, to considering the price of noble metals [3-5], it is more cost-effective to develop a coke resistant nickel - based catalyst, which would exhibit long-term stability. For instance, our previous work showed that the addition of ruthenium to the Ni/Al_2O_3 catalysts improved its activity and resistance towards carbon deposition during mixed reforming of methane [8]. The addition of cerium to nickel catalysts was also proven effective in increasing the stability of nickel catalysts. It was proposed that Ce favors the adsorption of CO_2 on the catalyst surface, accelerating the gasification of the CH_x species formed during the decomposition of methane [1,2].

Carbon deposition in the dry methane reforming occurs on the surface of catalysts by methane decomposition (Eq. (1)) and CO disproportion (Eq. (2)).

$$CH_4 \leftrightarrow C+2H_2,\ \Delta H=75\ kJ/mol \quad (1)$$

$$2CO \leftrightarrow C+CO_2,\ \Delta H=-172\ kJ/mol \quad (2)$$

The amount and type of carbon deposit depend on the nature of the metal surface, CH_4/CO_2 ratio in the feed, and the operating temperature [3]. In general, five distinct types of carbon deposits can be distinguished: (i) C_α - adsorbed atomic carbon (surface carbide), (ii) C_β - polymeric films and filaments (amorphous), (iii) C_v - whiskers/fibers/filaments (polymeric, amorphous), (iv) C_γ - nickel carbide (bulk), and (v) C_c - graphitic platelets and films (crystallite) [4]. When the reforming of hydrocarbon is performed under low temperatures (below 500 °C), adsorbed hydrocarbon species on the surface of catalyst can accumulate and then slowly polymerize into an encapsulating film, blocking and deactivating the catalyst. Above 450 °C, the atomic carbon diffuses through the metal crystal and, after reaching saturation level, precipitates out in the form of filaments. This type of carbon does not deactivate the nickel surface but rather causes mechanical failure by lifting the metal crystallite from the catalyst surface. At high temperatures (above 600 °C), pyrolytic coke formed by the thermal cracking of hydrocarbons may encapsulate and deactivate the catalyst particle [5].

It has been reported that under the conditions of dry reforming of methane (700-900 °C), a carbon deposit can be formed on the surface of catalyst in the form of whiskers/filaments (C_v) and gra-

†To whom correspondence should be addressed.
E-mail: oleksandr.shtyka@p.lodz.pl

phitic films (C_c) [6]. These forms of carbon, under certain reaction conditions, can be gasified by components of biogas and by gaseous products of its reforming. The aim of this work was to investigate the reactivity of carbon deposits towards different gases (hydrogen, water, and carbon dioxide) and to develop a mechanism for removing the carbon deposit formed during the mixed reforming of methane process over Ni/Al_2O_3 catalyst.

EXPERIMENTAL SECTION

In our experiments, all chemical reagents were of analytical grade, obtained from commercial suppliers, and used without further purification.

1. Catalyst Preparation

Aluminum oxide was prepared by precipitation method from an aqueous solution of aluminum nitrate. Ammonia solution was used as a precipitating agent during preparation of $Al(OH)_3$ (at pH 9-10). After 24 hours, the resulting mixture was filtered and washed with deionized water until the pH of the solution of filtrate reached the value 7. Next, the obtained mixture was dried at 100 °C for 12 h and calcined for 4 h in an air atmosphere at 500 °C.

The monometallic Ni support catalyst was prepared by wet impregnation method. The corresponding amount of the aqueous precursor solutions was dropwise added to $Al(OH)_3$ and left under ambient conditions for 24 h. Next, the water was evaporated under vacuum. Finally, the prepared samples were dried and then calcined at 500 °C for 4 h. The nominal metal content in the obtained catalysts was 20 wt%

2. Characterization Methods

SEM measurements were performed using a scanning electron microscope HITACHI, equipped with an energy dispersive spectrometer EDS (Thermo Noran). Raman measurements were carried out with use of Jobin Yvon T64000 triple grating Raman spectrometer (Ar laser excitation lines - 514.5 and 488 nm) with a spectral resolution below 1 cm^{-1}, and Fourier transform Raman spectrometer MultiRAM (Bruker) equipped with Nd : YAG laser (excitation wavelength 1,064 nm) and with high-sensitivity Ge diode detector. The total organic carbon (TOC) content of the samples of was determined on a TOC 5000A analyzer (Shimadzu, Japan). Carbon was burnt to CO_2 at 900 °C. A nondispersive infrared gas analyzer was used as a detector in all of the measurements. The instrument was calibrated with the use of pure glucose.

Nitrogen adsorption isotherms of catalyst and support were obtained at −196 °C using a Sorptomatic 1900 (Carlo Erba Instruments). The samples were previously outgassed at 300 °C and equilibrated under vacuum for at least 4 h before measuring the adsorption-desorption isotherm. Specific surface areas were evaluated from the measured monolayer capacity (Brunauer-Emmett-Teller method) using a range of relative pressure from ~0.05 to 0.33 and the value for nitrogen cross-section 0.162 nm^2. The pore size distribution was calculated by the Dollimore and Heal (DH) method from the desorption branch of the isotherm.

Room temperature X-ray powder diffraction patterns were collected using a PANalytical X'Pert Pro MPD diffractometer in Bragg Brentano reflection geometry. The diffractometer was equipped with Cu Kα radiation source (λ=1.5418 Å). Data was collected in the 2θ range of 5°-90° with a step size of 0.0167° and exposure per step of 27 sec. Because the raw diffraction data contain some noise, the background during the analysis was subtracted using the Sonneveld, E. J. and Visser algorithm. The data were then smoothed using a cubic polynomial function. The average of size metal particles was calculated using the Scherrer equation.

The temperature programmed surface reaction was carried out in a quartz reactor in the temperature range from 25 up to 900 °C with a linear heating rate of 10 °C/min. Carbonized samples (weight about 0.1 g) were reduced/oxidized in hydrogen (5%H_2-95%Ar and 100%H_2), carbon dioxide (5%CO_2-95%Ar), H_2O (5%H_2O-95%Ar) and O_2 (5%O_2-95%Ar) stream with a volumetric flow rate of 30 cm^3/min, respectively. The evolution of the gaseous products was analyzed as a function of temperature using mass spectrometer. Prior to the measurements, each sample was heated in an Ar atmosphere at 100 °C for 1 hour.

The methane cracking/reforming and carbon monoxide disproportionation reactions were investigated in a quartz reactor in the temperature range from 25 up to 900 °C with a linear heating rate of 10 °C/min. Prior to the measurements, the catalyst was reduced in-situ in hydrogen stream (5%H_2-95%Ar) at 700 °C for 1 hour. Then, the sample (weigh about 0.1 g) was exposed to either methane (5%CH_4-95%He/ reaction mixture) or carbon monoxide (5%CO-95%Ar) streams. The volumetric flow of the reaction gases was 30 cm^3/min. The reaction products were analyzed using a mass spectrometer detector.

3. Catalytic Activity Tests

The reaction of dry reforming of methane was investigated in a flow-type quartz microreactor under atmospheric pressure at temperatures of 700 and 750 °C. In each test, about 0.4 g of catalyst was placed in the reactor. The composition of the reaction mixture in each test was as follows: $CH_4 : CO_2 : H_2 : H_2O : Ar$=2 : 2 : 1 : 0.9 : 1.25 (volumetric ratio). The gas of such composition (except argon and water) is formed during biological conversion of sugar industry wastes. The total flow of the reaction mixture was 100 cm^3/min. The catalytic activity was measured after preliminary stabilization for 0.5 h. The composition of gases before and after the reaction was measured using gas chromatographs equipped with thermal conductivity detectors.

Methane and carbon dioxide conversions were calculated using the following formulas:

$$K_{CH_4} = \left(\frac{W_{oCH_4} - \left(W_{iCH_4} * \frac{W_{oAr}}{W_{iAr}} \right)}{W_{oCH_4}} \right) * 100\%$$

$$K_{CO_2} = \left(\frac{W_{oCO_2} - \left(W_{iCO_2} * \frac{W_{oAr}}{W_{iAr}} \right)}{W_{oCO_2}} \right) * 100\%$$

where: W_iCH_4, W_iCO_2, W_iAr - corresponds to the average content of CH_4, CO_2 or Ar from three surface measurements originating from the injection of the reaction mixture at a given temperature,

W_o CH_4, W_o CO_2, W_o Ar - corresponds to the average of the CH_4, CO_2 or Ar standard from three surface measurements originating from the injection of the standard mixture.

Table 1. Catalyst and support properties

Samples	Average size of Ni particles, nm	Specific surface area, m^2/g	Pore size, nm
Al_2O_3	-	196	2.76-3.87
$20\%Ni/Al_2O_3$	20	130	2.81-3.49

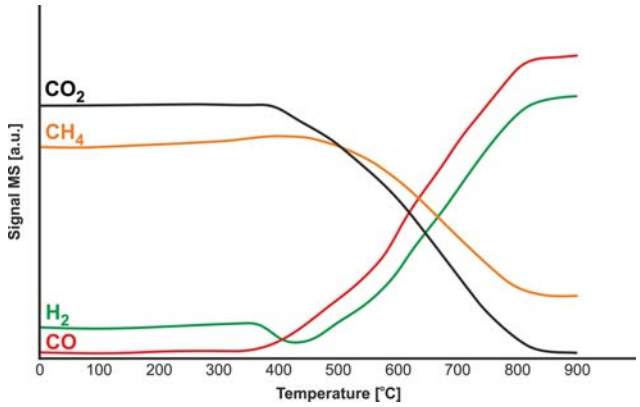

Fig. 1. TPSR profile for methane reforming over $20\%Ni/Al_2O_3$ catalyst.

RESULTS AND DISCUSSION

1. Catalytic Activity Measurements/Total Organic Carbon (TOC) Analysis

The physicochemical properties of prepared support and catalyst are presented in Table 1. The specific surface area of support was found to decrease from 196 to 130 m^2/g after deposition of nickel particles. This is related to a high concentration of low-surface-area metal phase. According to the XRD measurements, the average size of Ni particles was about 20 nm.

The TPSR measurements in the gas mixture (Fig. 1) showed that the methane reforming started at a temperature above 400 °C. It is clearly seen that below this temperature, the concertation of carbon dioxide was gradually decreasing followed by a subsequent increase in carbon oxide concentration. This effect was accompanied by prominent uptake of hydrogen and release of methane in the same temperature range. Such results imply that before methane reforming started, some amount of carbon dioxide was already converted into carbon monoxide, which was then hydrogenated to methane [7].

The TOC analysis of catalyst after 3 h of methane reforming showed that the amount of carbon deposit was the lowest at temperature 650 °C (Table 2). However, it was primarily due to the low conversion of methane equal to 20%. With further increase in temperature, the conversion of methane increased to 53 and 81% at 700 and 750 °C, respectively. Also, the catalyst investigated at 750 °C was characterized by a low concentration of carbon deposit, as indicated by the TOC analysis. This implies that the high temperature favors the gasification of carbon deposited on the surface of catalyst, which also could be a reason for its improved activity in the studied reaction.

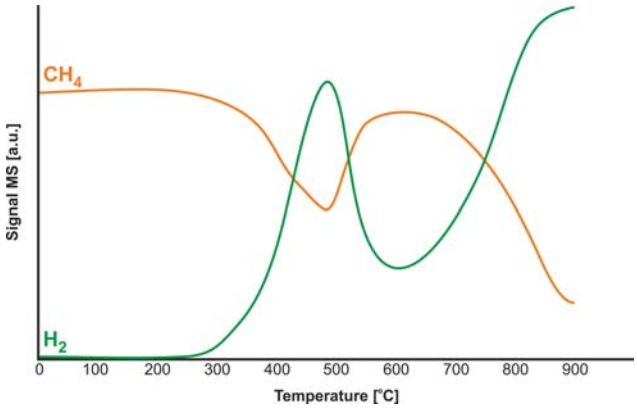

Fig. 2. TPSR profile for methane decomposition over $20\%Ni/Al_2O_3$ catalyst.

2. Coking Reactions

The carbon deposit on the surface of Ni/Al_2O_3 can be formed as a result of methane decomposition and/or CO disproportionation. Non-catalytic thermal decomposition of methane requires temperatures above 1,200 °C, while catalytic decomposition can proceed in the range of 600-800 °C. The result of temperature programmed decomposition of methane over $20\%Ni/Al_2O_3$ catalyst (Fig. 2) showed that methane started to decompose at about 300 °C. Next, the rate of reaction gradually increased with an increase in temperature, which is consistent with Le Chatelier's principle. The sharp fall in the rate of methane decomposition observed at 600 °C was due to reversible deactivation of the catalyst as a result of intensive carbon deposition on its surface. This carbonaceous deposit, however, was etched by hydrogen at a higher temperature. Consequently, this led to further increase in the rate of methane decomposition and hydrogen formation. A similar observation was reported by Rahman et al. who investigated the activity of $5\%Ni/\gamma$-Al_2O_3 in methane decomposition process. They reported that the fastest deactivation of catalyst was observed from 600 to 650 °C due to intense carbon deposition process [8].

The second reaction leading to the formation of a carbon deposit is the reversible CO disproportionation (Fig. 3). According to the TPSR results, the reaction occurs over a wide range from 200 to 800 °C. The maximum rate of CO consumption was observed at

Table 2. The catalytic performance of Ni/Al_2O_3 catalyst in the mixed reforming of methane

Catalyst/ Reaction temperature	The amount of carbon deposit after 3 h of the reaction, %	Conversion of CH_4 after 3 h of reaction, %	Conversion of CO_2 after 3 h of reaction, %
$20\%Ni/Al_2O_3$/650 °C	2.8	20	24
$20\%Ni/Al_2O_3$/700 °C	5.9	53	59
$20\%Ni/Al_2O_3$/750 °C	3.3	81	66

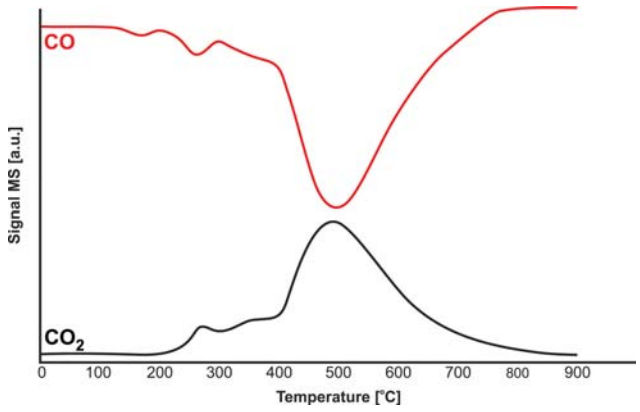

Fig. 3. TPSR profile for CO disproportionation over 20%Ni/Al_2O_3 catalyst.

500 °C, followed by a gradual decrease at higher temperatures (>500 °C) due to thermodynamic limitations.

As can be seen, both methane decomposition and CO disproportionation are the major pathways for carbon deposition below 500 °C. Above 700 °C, however, methane decomposition is solely responsible for carbon deposition.

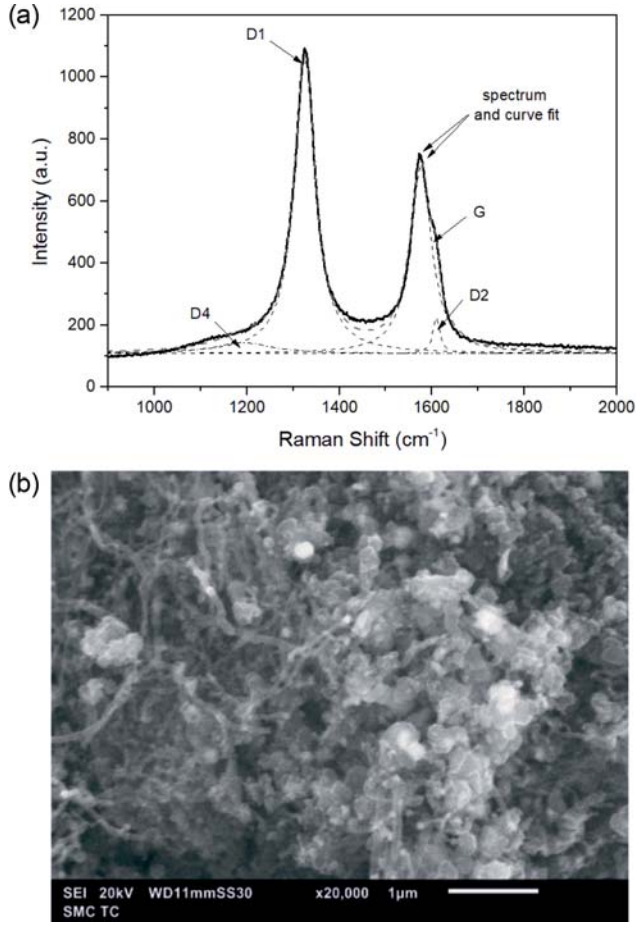

Fig. 4. SEM and Raman measurements of the 20%Ni/Al_2O_3 catalyst after mixed reforming of methane at 750 °C.

3. Morphology Studies of Carbon Deposits

The Raman spectrum (Fig. 4(a)) of the used catalyst exhibited two broad peaks with intensity maxima at 1,326 and 1,573 cm^{-1}, which were deconvoluted using a single Lorentzian fitting function. The result of the fitting procedure showed the presence of four peaks: G peak (1,575 cm^{-1}, ideal graphitic lattice), D1 peak (1,324 cm^{-1}, disordered graphitic lattice), D2 peak (1,610 cm^{-1}, ideal graphitic lattice), and D4 peak (1,200 cm^{-1}, disordered graphitic lattice). No D3 peak (1,500 cm^{-1}), related to the amorphous carbon, was observed. The obtained Raman spectrum is typical for carbon nanotubes [9]. This is in good agreement with SEM results. The microscope analysis of the surface of used catalyst revealed carbon in the form of filaments (Fig. 4(b)). No other forms of carbon were detected due to apparatus limitation.

4. Reactivity of Carbon Deposits Towards Different Gases

4-1. Oxygen

Temperature-programed surface reactions in oxygen atmosphere were performed in an attempt to distinguish the different types of carbon deposits formed on the surface of the catalysts. The TPSR profile (Fig. 5) showed two oxygen consumption effects, one wide peak located in the temperature range of 230-450 °C and another prominent peak with a maximum of about 670 °C. The latter effect was accompanied by noticeable evolution of carbon oxides, indicating the oxidation of inactive form of carbon deposit. The former effect, on the other hand, was not followed by significant formation of carbon oxides. Therefore, the oxygen consumption effect was probably connected with oxidation of negligible amounts of polymeric or encapsulated carbon and then nickel particles.

4-2. Hydrogen Mixtures

As observed earlier, hydrogen gasifies the carbon deposit on the surface of catalyst at high temperatures (Fig. 2). Indeed, nickel catalysts are considered to be one of the most effective in methanization processes. For example, Ma and Yang et al. reported that the supported Ni particles can catalyze the gasification of carbon support at the temperature as low as 510 °C [10,11]. Yamasaki et al. found that an amorphous alloy of Ni-25Zr-5Sm effectively catalyzed the hydrogenation of carbon dioxide (with the conversion of about 90%) at 300 °C [12]. However, during TPSR measurements

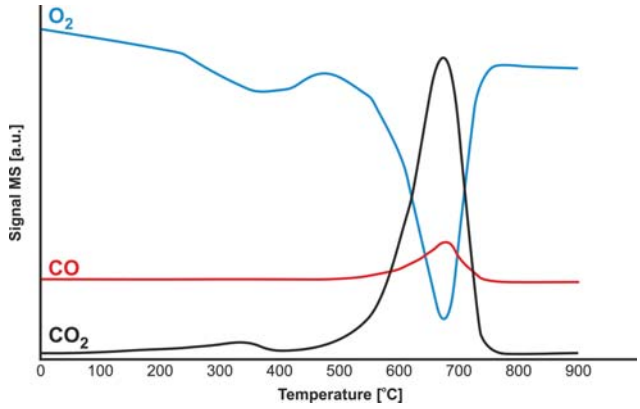

Fig. 5. TPSR of oxygen (5%O_2-95%Ar) stream with carbon deposited on the surface of catalyst after mixed reforming of methane at 750 °C.

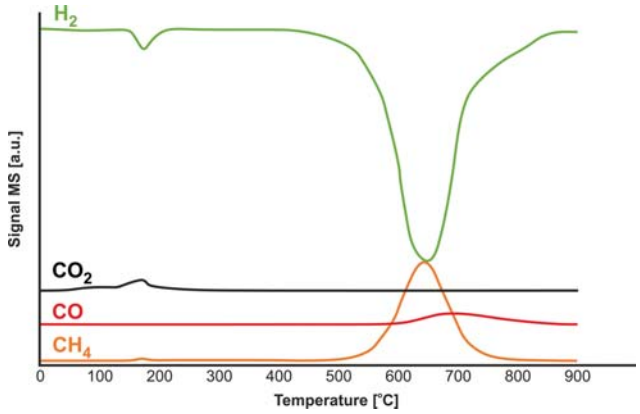

Fig. 6. TPSR of pure hydrogen with carbon deposited on the surface of catalyst after mixed reforming of methane at 750 °C.

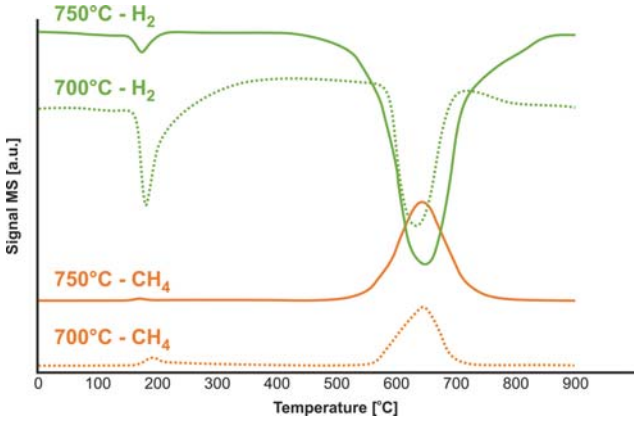

Fig. 7. TPSR of pure hydrogen with carbon deposited on the surface of catalyst after reforming of methane at 700 °C and 750 °C.

in hydrogen stream (5%H_2-95%Ar) no detectable uptake of hydrogen was observed over the whole investigated temperature range (not shown). The TOC analysis also confirmed the same amount of carbon on the surface of catalyst before and after gasification in the hydrogen stream (Table 2). Such results are in contradiction with those observed previously as well as with scientific literature [13]. This is probably due to the low partial pressure of hydrogen in the gas mixture, which is a crucial parameter for hydrogenation processes. Particularly, it was reported that gasification rates increase profoundly with increasing hydrogen partial pressure [14]. Therefore, the same TPSR measurements were performed but in pure hydrogen gas (99.99% H_2). The obtained TPSR spectra (Fig. 6) showed two peaks associated with hydrogen consumption, namely, low-temperature peak at 200 °C and high-temperature peak at 650 °C. These peaks are followed by formation of methane at the same temperatures and, therefore, the observed effects can be ascribed to the methanation processes. Particularly, the high-temperature effect is connected with the reduction of either filamentous or encapsulated carbon. The low-temperature effect (below 200 °C) is usually assigned to the gasification of chemisorbed carbon species [15].

However, according to the obtained results, the formation of methane at this temperature was preceded by the evolution of carbon dioxide and adsorbed water in the same temperature region. Therefore, the methane probably originated from the reduction of carbon dioxide, which was previously adsorbed during the reaction and/or was formed as a result of oxidation of active carbon species by adsorbed water. The comparison of TPSR spectra of catalysts after the reaction at 700 and 750 °C (Fig. 7) showed that the former had a higher amount of active carbon species, while the second sample possessed higher concentration of inactive carbon.

Both samples were characterized by the absence of any detectable amount of carbon deposit after TPSR in pure hydrogen (Table 3).

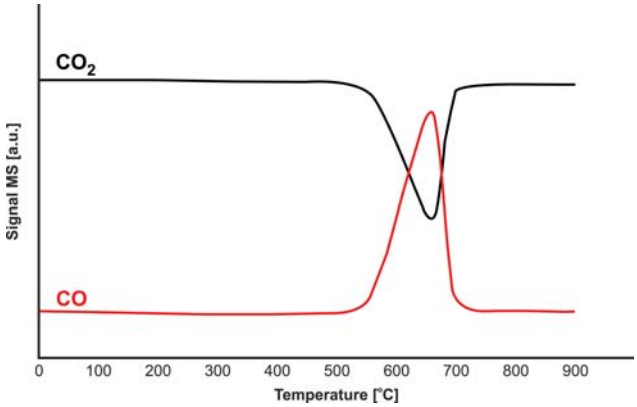

Fig. 8. TPSR of carbon dioxide (5%CO_2-95%Ar) stream with carbon deposited on the surface of catalyst after mixed reforming of methane at 750 °C.

4-3. Carbon Dioxide

The TPSR measurements in CO_2 mixture (5%CO_2-95%Ar) showed one prominent CO_2 consumption peak at about 670 °C (Fig. 8). This effect was accompanied by simultaneous evolution of carbon monoxide, which implies the complete gasification of carbon according to the following equation:

$$C+CO_2 \leftrightarrow 2CO, \qquad \Delta H=172\ kJ/mol \tag{3}$$

Similar results were reported by Tamai et al. It was reported that Ni catalyst exhibited high activity in gasification of carbon with carbon dioxide at the temperature as low as 550 °C [16].

4-4. Water Vapor

As can be seen from the evolution of hydrogen, the gasification

Table 3. The amount of carbon deposit on the surface of catalyst after mixed reforming of methane and after gasification during TPSR

Sample/The amount of carbon deposit	After mixed reforming of methane, %	After gasification in H_2 mixture, %	After gasification in pure H_2, %	After gasification in CO_2 mixture, %	After gasification in H_2O mixture, %
20%Ni/Al_2O_3 - 700 °C	5.9	5.9	0	0	0
20%Ni/Al_2O_3 - 750 °C	3.3	3.3	0	0	0

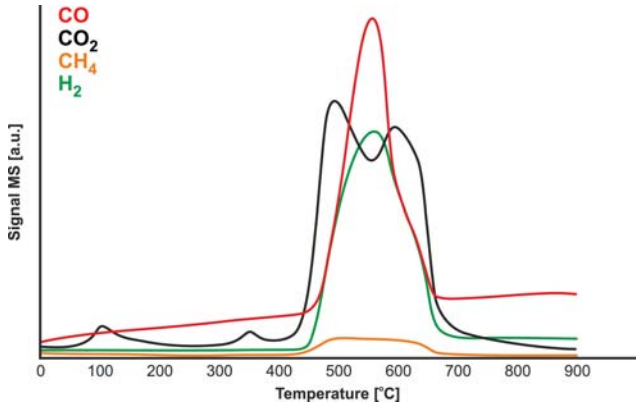

Fig. 9. TPSR of water vapor (5%H_2O-95%Ar) steam with carbon deposited on the surface of catalyst after mixed reforming of methane at 750 °C.

of carbon deposit with steam occurred in a wide range from 430-700 °C (Fig. 9). The process was accompanied by the formation of methane and both carbon mono- and dioxide. Moreover, some amount of carbon dioxide was probably converted into carbon monoxide above 600 °C due to reverse water gas shift reaction. The formed gas subsequently underwent hydrogenation to methane.

MECHANISM OF MIXED REFORMING OF METHANE

Based on the obtained results as well as literature review, a reaction mechanism of methane reforming was proposed (Fig. 10). The reaction mechanism is divided into three parts: methane decomposition (1), carbon dioxide dissociation (2) and water vapor dissociation (3). It is generally accepted that decomposition of methane first process through dissociative adsorption of methane on nickel active sites (1.1) followed by a series of dehydrogenation steps leading to elemental carbon (1.5) and hydrogen. The formed hydrogen atom can further recombine to form H_2 and desorb onto effluent gas steam (4.1-4.2), while carbon polymerizes and rearranges to form less active polymeric film and eventually encapsulates the catalyst surface (5.1-5.2). Also, the reactive carbon species dissolves through the nickel particles and diffuses through it until they precipitate in the form of filaments (5.3) [17]. The carbon dioxide adsorbs on nickel sites producing surface CO and oxygen atoms (2.1-2.2). The adsorbed CO can further dissociate to carbon (2.3) and oxygen, desorb (2.4), and react with another molecule of CO to form carbon and CO_2 (2.5). Also, CO molecule might react with hydroxyls (2.6) generated as a result of water dissociation (3) to produce carboxyl or formate intermediate (not shown), which subsequently decomposes into CO_2 and hydrogen. The formed carbon dioxide can either dissociate to form again CO or desorb (2.1). The adsorbed carbon species CH_{0-3} undergoes oxidation by atomic oxygen (from CO_2 and H_2O dissociation) and hydroxyl (H_2O dissociation) forming intermediates (6.1-6.2), which then decomposes yielding hydrogen and CO (6.3) [18]. These oxygenated intermediates can be also hydrogenated to methane as shown by reactions 6.4 and 6.5. As mentioned previously, the carbon deposit is formed via both methane dissociation and carbon dioxide dissociation routes. This carbon undergoes subsequent hydrogenation as well as oxidation by adsorbed hydroxyl and oxygen. The hydrogenation of carbon is basically a reverse methane dissociation process that occurs via formation of $CH_{(0-3)}$ species above 550 °C (1.5-1.1). The oxidation of carbon either by oxygen (2.3) or hydroxyl species (6.6) results in the formation of CO, which under reaction conditions can be desorbed (2.4), converted into CO_2 (2.6) and/or methane (6.3-6.4 or 2.3, 1.5-1.1). The rate-determining step of the

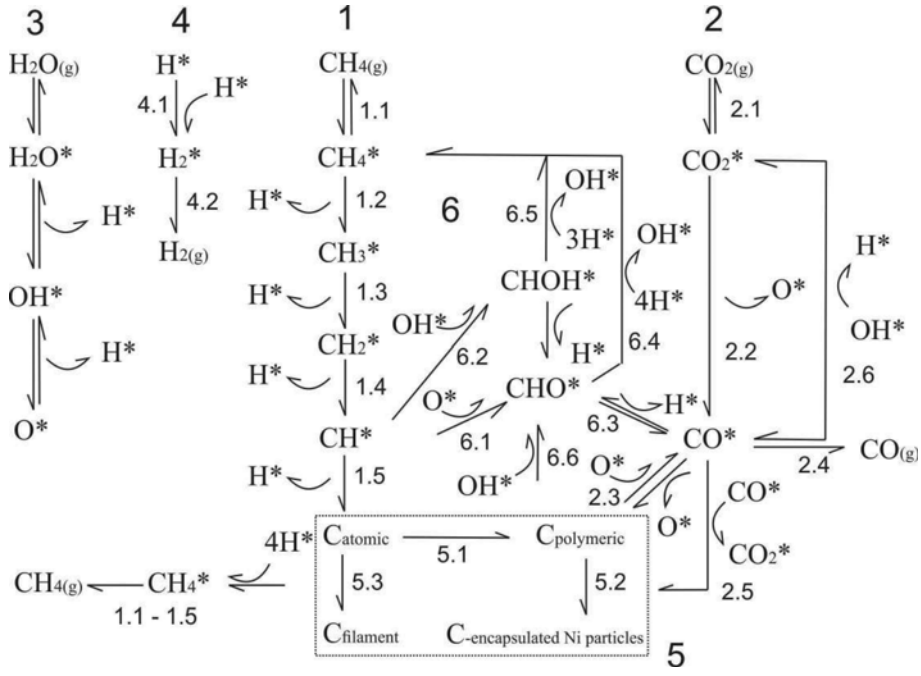

Fig. 10. Reaction pathways of mixed methane reforming.

whole process is thought to be a CH_4 dissociation into CH_3 and H. However, it was shown that it may be the case only at low temperatures, while at high temperatures the rate-determining step is the oxidation of hydro-carbonated species. The stability of catalyst in this process significantly depends on the presence of surface H and O atoms, which can help to eliminate the carbon deposit on the surface of catalyst. Indeed, the oxygen and hydrogen effectively removed the carbon species above 550 °C. However, water vapor proved to be more efficient in the gasification of carbon, which may be due to a better adsorption of water on the surface of catalytic support (i.e., aluminum oxide).

CONCLUSIONS

The formation of carbon deposit on the surface of catalyst during methane reforming at a temperature above 700 °C occurs via methane decomposition. The active form of carbon is readily gasified at low temperatures irrespective of gasification agents, while elimination of inactive ('graphitic') carbon form requires temperatures as high as 450-500 °C. The results of TOC analysis confirmed that high temperatures facilitate the removal of carbon deposit. The elimination of carbon occurs via hydrogenation to methane (if a sufficient amount of hydrogen is present) as well as through oxidation by oxygen atoms and/or hydroxyls to CO, which further can be converted either to methane and carbon dioxide or desorbed onto effluent gas steam. Among all investigated gasification agents, the water vapor was found to be the most efficient in removing the carbon deposit which can be explained by a good adsorption of water vapor on the surface of aluminum oxide.

ACKNOWLEDGEMENT

This work was partially funded from NCBiR - Grant no. BIOSTRATEG2/297310/13/NCBiR/2016.

LIST OF ABBREVIATIONS

SEM : scanning electron microscope
EDS : energy dispersive spectrometer
TOC : total organic carbon
TPSR : temperature programmed surface reaction
C_α : carbon deposits - adsorbed atomic carbon (surface carbide)
C_β : carbon deposits - polymeric films and filaments (amorphous)
C_v : carbon deposits - whiskers/fibers/filaments (polymeric, amorphous)
C_γ : carbon deposits - nickel carbide (bulk)
C_c : carbon deposits - graphitic platelets and films (crystallite)

REFERENCES

1. C. Dazaa, A. Kiennemann, S. Morenoa and R. Molina, *Appl. Catal. A: Gen.*, **364**, 65 (2009).
2. C. Daza, J. Gallego, F. Mondragon, S. Moreno and R. Molina, *Fuel*, **83**, 592 (2010).
3. P. Schulz, M. Gonzalez, C. Quincoces and C. Gigola, *Ind. Eng. Chem. Res.*, **44**, 9020 (2005).
4. C. H. Bartholomew, *Appl. Catal. A: Gen.*, **212**, 17 (2001).
5. J. R. Rostrup-Nielsen, in: J. R. Anderson and M. Boudard, (Eds.), *Catalysis, Science and Technology Springer*, New York (1984).
6. E. Solh, Dry Reforming of Methane in a Fast Fluidized, Ph.D. Thesis, London: University of Western Ontario (2002).
7. H. Wu, Y. Chang, J. Wu, J. Lin, I. Lin and C. Chen, *Catal. Sci. Technol.*, **5**, 4154 (2015).
8. M. Rahman, E. Croiset and R. Hudgins, *Top. Catal.*, **37**, 137 (2006).
9. S. Rebel, A. Guedes, M. Szefczyk and A. Pereira, *Phys. Chem. Chem. Phys.*, **18**, 12784 (2016).
10. H. Yang, S. Songa, R. Rao, X. Wang, Q. Yu and A. Zhang, *J. Mol. Catal. A: Chem.*, **323**, 33 (2010).
11. X. Zhao, Y. Lu and W. Liao, *J. Fuel. Chem. Technol.*, **43**, 581 (2015).
12. M. Yamasaki, M. Komori, E. Akiyama and H. Habazaki, *Mater. Sci. Eng. A*, **267**, 220 (1999).
13. J. McCarty, P. Hou, D. Sheridan and H. Wise, *SRI Int.*, **202**, 253 (1983).
14. M. Saboktakin, R. Tabatabaie, A. Maharramov and M. Ramazanov, *Synth. Commun.*, **41**, 1455 (2011).
15. J. McCarty, P. Hou, D. Sheridan and H. Wise, *Am. Chem. Soc.*, **202**, 253 (1983).
16. Y. Tamai, H. Watanabe and A. Tomita, *Carbon*, **15**, 103 (1997).
17. D. Trimm, *Chem. Eng. Process.*, **18**, 137 (1984).
18. L. Maier, B. Schadel, K. Herrera Delgado, S. Tischer and O. Deutschmann, *Top. Catal.*, **54**, 845 (2011).